

Buckling in Wurtzite-Like AlN Nanostructures and Crystals: Why Nano can be Different

C. J. F. Solano, A. Costales, E. Francisco, A. Martín Pendás, and Miguel A. Blanco¹ and K.-C. Lau, H. He, and Ravindra Pandey²

Abstract: The buckling of hexagonal layers in bulk and nanostructures of AlN is analyzed in the framework of atomistic and first principles techniques. At ambient conditions, the wurtzite structure (B4) of AlN consists of buckled hexagons. On the other hand, a non-buckled B_k structure is found to be metastable at zero pressure, being favored at higher pressures. It is suggested that the energy ordering of B4 and B_k may change in finite systems; an assertion tested in this study by considering finite slabs, nanobelts, and nanorings, and comparing the results with the previous studies on small clusters, and periodic nanostructures. We find that the buckling in finite systems is much smaller than that in the bulk material, with N atoms sticking out in the first layer, followed by an even smaller opposite buckling of the next layer, and negligible buckling of the inner layers. All the structures considered present some degree of symmetry, usually a σ_z symmetry plane, so that buckling is opposite on both sides of the finite system and thus the dipole moment is quenched. Periodic nanostructures display no buckling, a fact that is related with their ability to model the inner part of the system, neglecting geometric surface effects. It is suggested that the zero-dipole and negligible buckling present in the small size regime will lead to buckled hexagons in larger finite systems, similar to the bulk behavior, thus introducing a change in the size dependence of their structural and electronic properties.

Keyword: Buckling, wurtzite, AlN, semicon-

ductors, bulk, slabs, nanostructures, clusters.

1 Introduction

The wurtzite structure (*Strukturbericht* symbol B4) is the lowest energy one for many binary compounds at ambient conditions, ranging from ionic-like oxides (BeO, ZnO), to semiconductors (AlN, GaN, SiC). For an AB compound, it can be described (see Fig. 1) by alternating layers (abab...), each layer consisting of a lattice of hexagons with alternating A and B atoms on their vertices. The hexagons are *buckled*, that is, one of the types of atoms (say A) is above the average layer level, and the other (say B) below it. Successive layers alternate the positions of A and B atoms and the direction of the buckling, so that above the position of an A atom in the first layer, in which it was above the average layer level, sits a B atom in the second layer which is below the average level for that second layer. Thus, in addition to the three intralayer A–B bonds, the buckling facilitates the formation of an extra interlayer A–B bond, giving a coordination index of 4 to both atoms in the structure. Using the $P6_3mc$ hexagonal space group, both atoms in the wurtzite phase will occupy position $2b$, $(1/3, 2/3, 0)$ (A atom) $(2/3, 1/3, z)$ (B atom). Notice that there is freedom along z at these positions, which are interchangeable, and so it is the difference in z that matters, not the proposed values of 0 and z . We will now use the z value to quantify the buckling of the structure. We note that the above description is somewhat different from that used by other authors, with atomic coordinates $(1/3, 2/3, 0)$ and $(1/3, 2/3, u)$ where $u = 1/2 - z$; this definition yields half layer at the bottom, one full layer in the middle, and another half layer at the top of the

¹Dpt. Química Física y Analítica, Universidad de Oviedo, Oviedo, Spain. Corresponding author: miguel@carbono.quimica.uniovi.es

²Department of Physics, Michigan Technological University, Houghton, MI, USA.

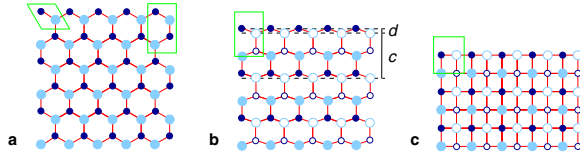


Figure 1: Structures of the phases discussed in the text: a) [001] view of B4 and B_k phases; b) [010] view of B4 phase; c) [010] view of the B_k phase. $A \equiv \text{Al}$ atoms are larger light circles, $B \equiv \text{N}$ atoms are smaller dark circles; empty circles represent atoms behind the projection plane. Unit cells shown, including both hexagonal (left) and orthorhombic (right) in panel a). Also shown in panel b) are the c lattice parameter, and the buckling $d = zc$.

unit cell. In this paper, we prefer the $(2/3, 1/3, z)$ coordinates because the unit cell will include two complete layers.

In the description used here, a $z = 1/4 - 1/(3(c/a)^2)$ value, combined with the ideal $c/a = \sqrt{8/3} = 1.632993$ ratio (thus $z = 1/8 = 0.125$), leads to a perfect tetrahedron coordination sphere. Despite first- and second-neighbors bearing a symmetric disposition around a given atom, each position is still affected by a non-zero electric field if the crystal bond is heteropolar. This makes each atom, occupying a polar position, acquire a different dipole depending on its polarizability; in order to equilibrate the forces thus introduced in the lattice, real crystals deviate from this ideal structure. For example, in the case of AlN, the values of $c/a = 1.6009$ and $z = 0.1128$ are at ambient conditions; thus, the tetrahedra are somewhat flattened, with the intralayer A–A distances being 1.3 % larger than the interlayer ones, and the hexagonal layer is further flattened, with the interlayer A–B bond being 2.5 % larger than the intralayer ones. However, in an ideal infinite crystal, neither these dipoles nor those due to the non-polar point-charge-like distribution are considered to introduce a surface energy, since the ideal crystal has no surfaces. This is not true, of course, for real macroscopic B4 crystals, which never have perfect [001] facets; the polar surface is usually reconstructed, compensating the

dipole which would lead to huge energies in the macroscopic regime. The situation is different for microscopically finite systems (as opposed to a macroscopic finite crystal): either slabs, formally infinite on the perpendicular plane, or clusters, completely finite, present a finite dimension along the polar z direction. The uncompensated charge distribution of a surface with the B4 structure leads to a finite surface energy which increases with the size of the system.

The situation in nanoscale systems can thus be different from the perfect crystal one. The dipole contribution to the surface energy will affect the structure of nanosystems in various ways. Since the main contribution comes from the buckling (an unbuckled situation will have zero dipole), this is the variable that we want to explore in the present study. There are other possible structural rearrangements; Morgan and Madden [Morgan and Madden (2007)], in a recent molecular dynamics simulation, have found nanoscale domains with opposing buckling resulting into no net dipole. However, this arrangement does not scale up to the macroscopic regime, in which the diffraction patterns do not show any domain structure. It will not be further pursued in our work though there is a possibility of its existence at the nanoscale regime. Our focus will thus be on the buckling of the layers; it has also been the subject of recent works by Allan's group on nanofilms [Freeman, Claeysens, Allan, and Harding (2006a,b)], which will be discussed along with our own results in Section 3.

Coming back to crystals, there are indeed other structures that come into play in AlN and related systems. First, application of the high pressure leads to a more compact, six-fold coordinated rock-salt type structure (B1). Then, there is the related, and always similar in energy, zinc-blende type structure (B3), which occurs at the ambient conditions for related materials like AlAs, AlP, or GaAs. Furthermore, there is yet another related structure referred to as the B_k structure (see Fig. 1) in which flat hexagonal layers (i.e., $z = 0$) exist (e.g. BN). This structure of BN is iso-electronic with the graphite structure consisting of hexagonal, flat layers, which are sometimes

called graphene-like sheets. The aromaticity of the hexagonal layers in graphite is sometimes assumed to be the main cause for the planarity in BN, although there is some controversy regarding the aromaticity of the layers in the latter case. What is nonetheless true is that, being flat, there is no dipole in the z direction. In fact, the B_k structure can be simply viewed as a distortion of the B4 structure in which the coordination has changed to either 5 if interlayer bonds are considered, or 3 if they are not considered. The B_k structure (i.e. $z = 0$) is a critical point in the energy surface corresponding to B4, since it displays a higher symmetry ($P6_3/mmc$), and it plays an important role in the high-pressure transformation from B4 into B1 in the group V nitrides [Cai and Chen (2007)]. The focus of this paper is to study how buckling is affected by various variables including pressure, size, and composition on systems of different scales: crystals, slabs, and nanostructures. In discussions, we will use results from the previous studies, and present new ones from our study to extract general conclusions. The rest of the paper is organized as follows. First, we will briefly describe the computational techniques employed in this study in Section 2. The main results will be presented and discussed in Section 3. Our conclusions will be given in Section 4.

2 Computational techniques

In order to secure a general behavior in crystals, slabs and nanostructures, as method-independent as possible, we have employed a wide range of methodologies to treat these systems studied. Even more, we will also use results obtained in our previous studies to further strengthen the conclusions of this one. Simulation of nanostructures is an actively developing field, in which multiscale methods are key [Ghoniem and Cho (2002); Shen and Atluri (2004); Tewary and Read (2004)].

First, we have employed periodic LCAO (linear combination of atomic orbitals) DFT calculations as implemented in Crystal03. The basis sets used were Pople's 6-31G*, reoptimized in the crystal, within the Generalized Gradient Approximation employing the Becke exchange

functional [Becke (1988)] and the Perdew-Wang correlation functional [Perdew and Wang (1992)] (GGA-BPW91). The code was used both in 3D periodic crystal calculations, and on 2D periodic slabs calculations. These results will be labelled Crystal3D and Crystal2D, respectively.

We have also employed *ab initio* derived pair potentials (PIIP, perturbed-ion interionic potentials), generated from accurate in-crystal electronic structure descriptions [Costales, Blanco, Francisco, Pandey, and Martín Pendás (2005)]. These have been thoroughly tested for AlN, and employed in other works [Costales, Blanco, Francisco, Solano, and Martín Pendás (2007)]. However, they do have the drawback of being spherically symmetric, thus not allowing the polarization of individual atoms. To account for this, we have also used shell-model potentials [Vail and Jiang (2006)], empirically derived, that we will label SM. This model allows polarization through the splitting of the atoms into core and valence-shell charges, linked by a spring-like potential. This model has proven to be very useful, specially in connection with lattice dynamics and phonon calculations. All of these potentials have been used to simulate 3D periodic crystals and nanostructures, by means of the pairpot3 [Pendás (1996)] and cluster [Francisco (2001-2004)] codes, respectively.

In addition to the new results in this paper, we will also include the results from our previous studies. Particularly, results in nanoclusters [Kandalam, Blanco, and Pandey (2001, 2002); Costales and Pandey (2003); Costales, Kandalam, and Pandey (2003); Costales, Blanco, Francisco, Martín Pendás, and Pandey (2006)], both employing DMol [Molecular Simulations, Inc. (1995)], a numerical basis sets LCAO code, and Gaussian [Frisch et al. (1998)], with 6-31G* basis sets, within the DFT-GGA-BPW91 framework. We will also mention the results of global optimizations of the structures of these nanoclusters employing the PIIP potentials [Costales, Blanco, Francisco, Pandey, and Martín Pendás (2005)]. These potentials have also been used in simulating nanocrystals [Costales, Blanco, Francisco, Solano, and Martín Pendás (2007)], and nanobelts

and nanorings [Solano (2006)] within a pseudoperiodic model, and also in previously unpublished full optimizations, with results that are also relevant to the present discussion. Similar computational methods can be found e.g. in [Ling and Atluri (2006); Park, Cho, Kim, Jun, and Im (2006)], whereas buckling is analyzed from a continuum point of view in [Baiz and Aliabadi (2006)].

3 Results and discussion

In this Section, we will present results corresponding to buckling in periodic and non-periodic systems. Although there is axial symmetry in which sublayers of Al and N atoms can be defined, the interlayer distances vary: both the distance between the Al and N sublayers in a given layer (d), and the distances between same-type layers, can have different values within a single multi-layer system, due to the lack of periodicity. Thus, for each system we have defined an average d value, together with an average c value as twice the average same-type interlayer distance, and so a $z = d/c$ value comparable across all systems can be defined (see Fig. 1). Although it may be more properly termed as Δz , as it is a difference in plane positions, and called average buckling or even z -equivalent buckling, d being the buckling proper, we will use the z symbol and refer to it as buckling for simplicity. It is important to notice that we define z as positive when the N sublayer is above the Al layer, negative otherwise. Although this is irrelevant for bulk systems, it is important in finite ones: positive z means the N atoms stick out of the system on its top part, negative z that Al sticks out, the reasoning being obvious for the intermediate and lower parts of the systems.

3.1 Bulk periodic systems

Let us start by studying how buckling affects bulk periodic systems. As previously stated, the B_k phase corresponds to the $z = 0$ value within the B4 phase configuration space. Thus, a most convenient way to understand how buckling takes place will be to plot energies against buckling. This is done in Fig. 2 which collects the results obtained from CRYSTAL, PIIP, and SM computa-

tional methods. Let us now focus on the PIIP values in Fig. 2. In addition to the E versus z curve (the one labelled $p = 0$), the change in the appropriate static potential, the Gibbs energy $G = E + pV$ (static conditions means $T = 0$ and neglect of zero-point vibrations, i.e. $U = E$), is plotted for different pressures, both positive and negative. Let us also recall that, owing to the symmetry plane present at the B_k $z = 0$ structure, the curves are symmetric for negative z , so that the B_k phase is always a critical point in the curve.

The B4 phase corresponds to the minimum at $z \simeq 0.11$ (see Tab. 1 for accurate values) for $p = 0$. This value is higher in energy than the $z = 0$ one by about 0.04 eV or 1 kcal/mol, contrary to the experimental observation of B4 as the most stable phase. However, the difference is, although opposite in sign, not large even in the most accurate Crystal3D calculations, of about 0.26 eV or 6 kcal/mol; hence, both phases are quite close in energy, a fact equally pointed by all the calculations reported in Tab. 1. In the PIIP rigid pair potential calculations, the B4 phase is more stable than B_k for pressures more negative than about -5 GPa, where both minima lie very close. This would be our estimate for the $B4 \rightleftharpoons B_k$ phase transition pressure, p_{tr} . For even more negative pressures, the B4 minimum becomes deeper and deeper, and the barrier from the B_k phase becomes smaller and smaller. This will continue down to a pressure (our estimate is about -35 GPa) in which the barrier will become zero. Below this pressure, the B_k phase will be a maximum against z and hence mechanically unstable. We shall call it to be the B_k phase instability pressure, $p_i(B_k)$. The same happens with the B4 phase if we increase the pressure above zero: the B_k minimum will be deeper and deeper, and the barrier from B4 to B_k will become smaller and smaller, up to about 20 GPa, in which B4 will turn into an inflection point, no longer with zero derivative, and hence unstable. Thus, all optimizations starting above this $p_i(B4)$ pressure will fall into B_k , $z = 0$.

The above results are quite general, as the different panels in Fig. 2 show. They slightly differ in the ΔE between the B_k and B4 phases at zero pressure, but the pressure evolution displays mostly

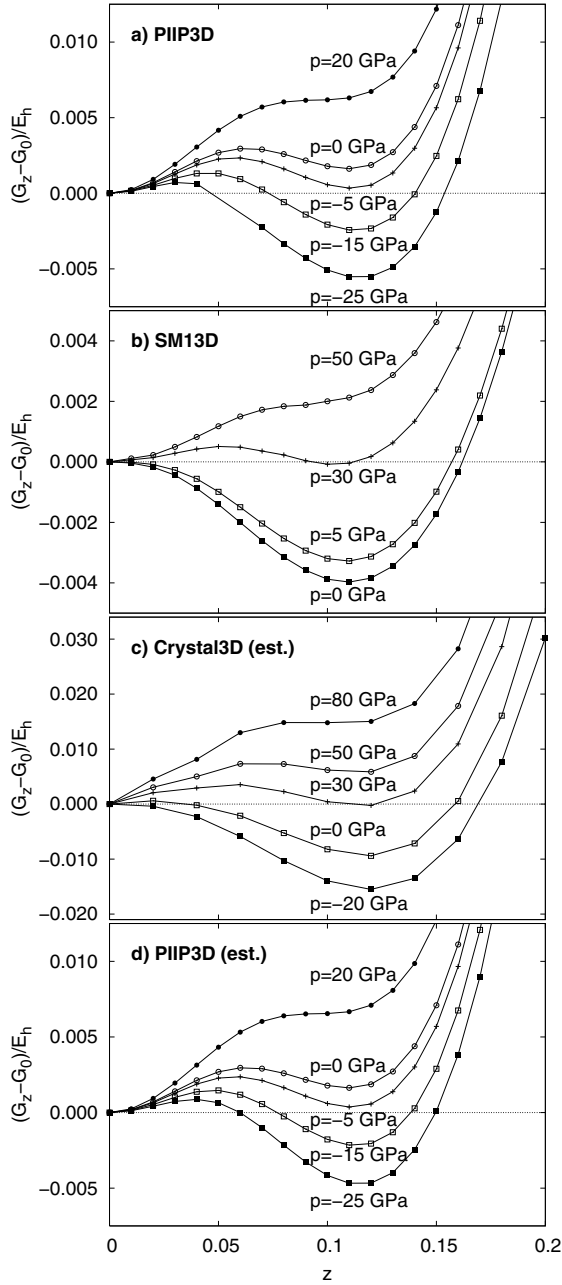


Figure 2: Static Gibbs energy ($G = E + pV$, in E_h) per unit formula as a function of buckling (z) for AlN at various pressures; the corresponding G_0 values at $z = 0$ have been subtracted to provide a common origin. a) PIIP values; b) SM values; c) Crystal3D values at $p = 0$, plus the $G_z(p) \simeq E_z(0) + pV_z(0)$ approximation; d) the same approximation applied to the PIIP values at $p = 0$.

Table 1: AlN B4 and B_k $p = 0$ bulk structural data, and $B4 \rightleftharpoons B_k$ static energy difference, ΔE .

	z (B4)	c/a (B4)	c/a (B_k)	$\Delta E/mE_h$
Exp.	0.1128	1.6009	—	—
PIIP	0.1098	1.5542	1.2000	-1.625
SM	0.1095	1.5680	1.3644	3.978
Crystal	0.1183	1.6033	1.2720	9.420

universal features. For example, the SM non-rigid potentials in panel b achieve a B4 phase lower than B_k at zero pressure (see also Tab. 1), having ($p_i(B_k)$, p_{tr} , $p_i(B4)$) values of about (0, 30, 50) GPa. In the case of the computationally expensive Crystal3D calculations, we have not optimized G for $p \neq 0$. However, we can estimate the pressure evolution by using $G_z(p) \simeq E_z(0) + pV_z(0)$, that is, assuming that E and V at fixed z do not change much with pressure (this can be tested for the PIIP potentials by comparing the real values in panel a and the estimate ones in panel d of Fig. 2). The Crystal3D values obtained with this approximation are presented in Fig. 2c. Again, the ($p_i(B_k)$, p_{tr} , $p_i(B4)$) values are about (-20, 30, 80) GPa. Thus, the actual values vary across different methodologies, but the main features and the ($p_i(B_k)$, p_{tr} , $p_i(B4)$) trends are universal.

The above picture seems to be general indeed, as there are indications pointing at it in several studies from the literature. For bulk solids, two different phase transition paths between B4 and B1 (rock-salt) have been proposed: a tetrahedral one, and a hexagonal one that passes through the B_k phase [Limpijumng and Lambrecht (2001); Miao and Lambrecht (2003); Saitta and Decremps (2004)]. Different materials favor one or the other, but both display first-order transition paths, that is, with the energy (or the appropriate thermodynamic potential) being minimal with respect to distortions orthogonal in configuration space to the transition path. Considering the hexagonal path, the authors have focused on the energy landscape at zero pressure, since their interest was on the $B4 \rightleftharpoons B1$ phase transition. Nevertheless, from [Limpijumng and Lambrecht

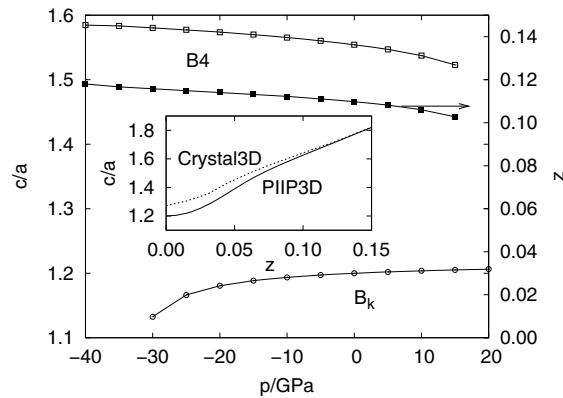


Figure 3: Variation of the structural c/a (B4 and B_k phases) and z (B4 phase) parameters with pressure for PIIP calculations on AlN. The inset compares the c/a versus z behavior of these calculations with the corresponding Crystal3D results.

(2001)] results one can conclude that for GaN the B_k phase is energetically unstable ($p_i(B_k) > 0$), while for MgO it is the B4 phase that is mechanically unstable ($p_i(B4) < 0$; we have estimated it to be about -10 GPa using out PIIP potentials); in both cases, $p = 0$ is not within the $[p_i(B_k), p_i(B4)]$ range of simultaneous stability of both phases. [Saitta and Decremps (2004)] results give p_{tr} values for ZnO, AlN, InN, GaN, and SiC, being 20, 25, 40, 182, and 198 GPa, respectively. On the other hand, [Cai and Chen (2007)] results include energy (enthalpy or Gibbs function) landscapes for several pressures, and so we can estimate the whole $(p_i(B_k), p_{tr}, p_i(B4))$ set of values from them by assuming suitable linear behavior against pressure of several energy differences. Thus, the values are $(-3, 27, 36)$ GPa for AlN, $(91, 142, 157)$ GPa for GaN, and $(18, 30, 34)$ GPa for InN. Thus, these authors confirm that the B_k phase is metastable at zero pressure for AlN, but not (by a large amount) for GaN. However, note that none of these transitions is experimentally available, since all of the computed systems have a lower transition pressure into the rock-salt B1 phase, six-fold coordinated; although the B_k intermediate could be kinetically found for AlN given the displayed barriers between B_k and B1, this cannot happen for the other two systems.

All of the above results show some trends: first, the $(p_i(B_k), p_{tr}, p_i(B4))$ values, related among them for a given material, increase with the trend of the material to be on the B4 phase, and decrease when the trend to be on the B_k phase increases. Given the results from the literature, it is clear that they appear to be related to the electronegativity differences. Thus, the p_{tr} values of [Saitta and Decremps (2004)] are larger for smaller electronegativity differences, for the highly ionic (large electronegativity difference) MgO even $p_i(B4)$ is below $p = 0$ in [Limpijumnong and Lambrecht (2001)], and the [Cai and Chen (2007)] values for the group-III nitrides are also in the inverse electronegativity difference order, $\text{AlN} < \text{InN} < \text{GaN}$ (although the extremely large values for GaN do not support proportionality). These trends can be viewed as chemical variations of a kind of driving force for the $B4 \rightarrow B_k$ transition: the larger this driving force is, the smaller the values in the $(p_i(B_k), p_{tr}, p_i(B4))$ set. However, given the spread of these values, it seems difficult to find scaling rules that make the trend truly universal. Also, one must keep in mind that, in many of these systems, the bulk B4 phase transforms directly into the B1 phase upon increasing pressure, and hence the usefulness of a universal bulk relation would be limited. In any case, indications of the driving force can be seen from the behavior of z and c/a with pressure; although these trends are displayed in the bulk materials, they can become more apparent and even experimentally observable in nanostructures. Among these, z and c/a vary almost linearly with p in the B4 phase, but they display a non-linear dependence at high pressure (see Fig. 3) as a precursor of the instability; although found for the PIIP calculations, the main $c/a(z)$ behavior (inset of Fig. 3) is similar in Crystal3D values, being the deviation larger near the B_k phase. In the latter phase, c/a is almost constant with p except for very low pressures, where again a curvature precursor of the instability is found.

3.2 Nanolayers

Let us now consider the case of nanolayers of AlN. These are systems periodic in two dimen-

sions, but finite in the other one. In order to study buckling, we will consider layers formed by stacking of the hexagonal graphene-like sheets described in Section 1, that is, [001] slabs. This system has been the subject of previous studies by Allan's group [Freeman, Claeysens, Allan, and Harding (2006a,b)], in which slabs of different materials are computed using Perdew and Wang exchange and correlation density functionals [Perdew and Wang (1992)] within a pseudopotential+planewaves scheme as implemented in castep. They found that non-buckled ($z = 0$) slabs were more stable than the buckled ones ($z \neq 0$) up to a given number of layers for each system: 4, 5, 6, 9, 12, and > 15 for SiC, ZnS, GaN, ZnO, AlN, and BeO, respectively. Notice that graphene-like, flat sheets are more persistent for the more ionic, not the more covalent, systems, contrarily to what covalent graphite itself might indicate. Let us recall that aromaticity (or double-bond character) is only important on bonds between second-period atoms of the principal groups, like those in graphite and (perhaps) BN (BeO being highly ionic is not expected to display any aromaticity), but not when third-period atoms are involved. Hence, none of the systems considered is aromatic, and so the graphite-like structure is not favored in this respect. In fact, there is a correlation between the maximum number of layers that stay non-buckled and the difference in Pauling's electronegativities, that is mostly linear except for AlN (BeO stays non-buckled [Freeman, Claeysens, Allan, and Harding (2006a)]): the more ionic a system is, the better it stabilizes non-buckled slabs. Exceptionally, AlN displays a larger stabilization of non-buckled slabs than its electronegativity difference may predict (it lies in between GaN and ZnO, whereas it stabilizes 12 layers as compared to 6 and 9 of GaN and ZnO, respectively). This is in agreement with the trend obtained for bulk systems, where the electronegativity difference increase led to smaller ($p_i(B_k)$, p_{tr} , $p_i(B4)$) values, and hence to a larger preference for the B_k structure. There is another striking fact in this direction: the buckled systems display metalization in the surface layers due to electron transfer from the N-terminated surface (2/3 from Al,

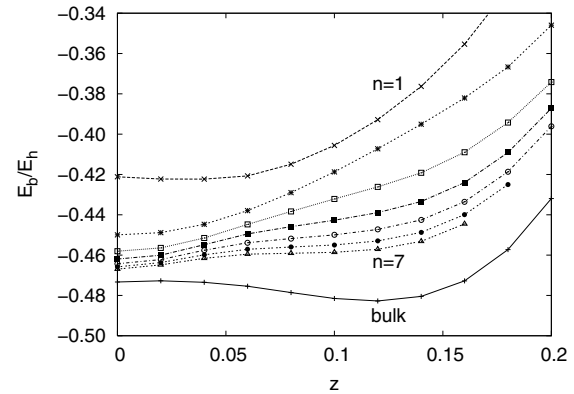


Figure 4: Crystal2D AlN slabs binding energy (E_b , in E_h) as a function of buckling (z) for different numbers of layers in the slab (n). The corresponding Crystal3D bulk binding energy after optimization of the structure with fixed z values is included for comparison. The geometry of the slabs is fixed to the corresponding z value bulk one.

1/3 from N) to the cations of the Al-terminated surface, according to a Mulliken analysis [Freeman, Claeysens, Allan, and Harding (2006b)], whereas the non-buckled systems remain insulating. Clearly, the metalization becomes easier when the electronegativity difference becomes smaller, hence the above correlation.

We have also performed slab calculations in AlN, labeled as Crystal2D (see Section 2), to analyze how their energy changes as a function of buckling and slab thickness. Fig. 4 shows the energy change with respect to both variables. Since the slab is non-periodic in the perpendicular direction, we cannot optimize inter-layer distances for a fixed z value, so we have sampled the z dependence by computing slabs fixed at the perfect crystal geometry for a given z value. Due to this restriction, the single-layer slab has a spurious minimum with $z \neq 0$, which disappears upon optimization (see below). Apart from this, all other systems studied display a minimum at $z = 0$, corresponding to B_k -like non-buckled slabs. There is a curvature change near the $B4$ buckling in slabs with $n > 1$, which is close to developing a minimum for $n = 7$. Unfortunately, we have not been

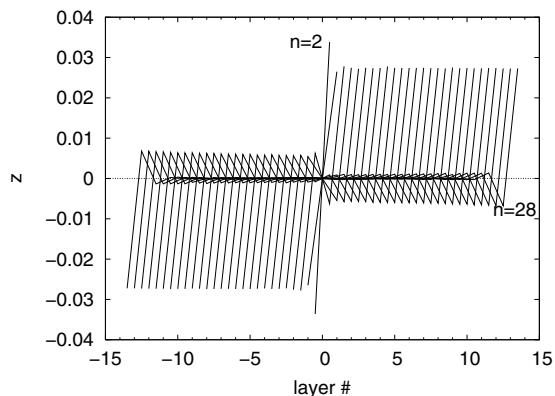


Figure 5: Crystal2D buckling for the different layers of B_k -like optimized AlN slabs with sizes up to $n = 28$. Owing to the σ_z symmetry plane, layer numbering is as follows: for n odd, the central one is layer 0, the rest being assigned positive and negative integers; for n even, the two central layers are labelled layer 1/2 and layer $-1/2$, the rest being labelled with half-integers so as to not overlap with those of the thinner slabs.

able to converge the SCF procedure in that region for larger slabs, but it seems that the sequence will continue by forming a minimum corresponding to B4 slabs, and that minimum will gradually become lower in energy than the $z = 0$ B_k -like slab minimum, finally leading to the bulk behavior displayed also in the graph (see the discussion in the previous Subsection).

We have also performed full slab optimizations from different starting geometries: that of the layers of the B4 bulk crystal, and that of layers of the B_k bulk crystal. Given the trends in the curves in Fig. 4, all of the former that we were able to converge (up to $n = 3$ layers) lead to the same minimum as the B_k -like ones, having a structure very close to the latter. The optimizations starting at the B_k geometry were performed up to $n = 28$, always finding a minimum close to that structure; this is not surprising, since the bulk B_k structure is a metastable minimum at $p = 0$ (see Fig. 2 panel c and Fig. 4). Regarding the buckling, Fig. 5 depicts its value for the different layers of these optimized structures. All of them have a σ_z symmetry plane, and the central layers of odd- n slabs

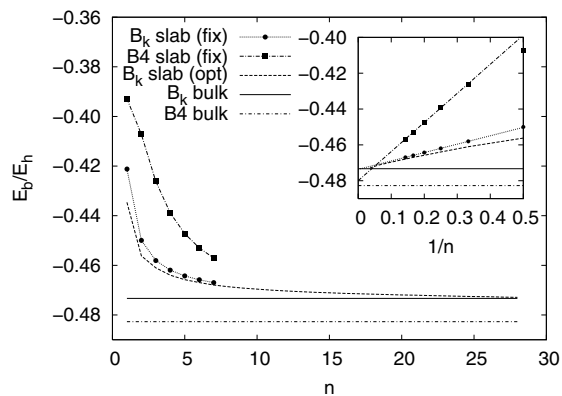


Figure 6: Crystal2D binding energy per unit formula (E_b , in E_h) versus number of layers (n) of different buckled (B4) and non-buckled (B_k) AlN slabs, together with the bulk limits. Data labelled fix corresponds to unit cells fixed at their Crystal3D optimum geometries, opt to a full optimization of the slab's geometry. The inset shows the trends against $1/n$ together with linear approximations.

present no buckling. It is apparent that, except for the smallest $n = 2$ and $n = 3$ slabs, all of the others have a converged structure, in which the upper layer has $z \simeq 0.027$ buckling, the next one $z \simeq -0.006$, the third one around $z \simeq 0.001$, and the inner ones have negligible buckling. This sequence is repeated symmetrically in the bottom layers, with opposite signs: N atoms stick out in both surfaces, and the total dipole moment is zero, owing to the symmetry plane. It is worth noting that this plane is not imposed in the optimizations starting at B4-like slab geometries, but a consequence of the optimization. Since we do not have converged results at large thickness, we do not know if it remains true up to the crossover of stabilities of B_k -like and B4-like slabs.

In order to locate the crossover of stabilities, Fig. 6 depicts the energy results of both types of slabs with geometries fixed at those of the corresponding bulk B_k and B4 optimized geometries (fix curves) and the B_k -like optimized ones described above (opt curves). It is plain to see that the fix curves approach one another, and that optimization does not introduce a very large energy

change. Hence, an extrapolation of the trends of the fixed-geometry curves can give a good estimate of the crossover. This is shown in the inset, presenting energies as a function of $1/n$, the reciprocal of the slab's thickness. The fixed-geometry data, after trimming the lowest (usually out-of-trend) n values, fit very accurately straight lines, with r^2 values better than 0.999 in both cases, that cross at $n = 18.24$. The B4-like one crosses the B_k optimized values around $n = 20.26$, however, and so we estimate the crossover to be 18 ± 2 . This is somewhat larger than the [Freeman, Claeysens, Allan, and Harding (2006a)] value of 12, but it displays a reasonable agreement.

3.3 Finite clusters

Let us now consider small clusters removing the effects of periodicity. The smallest cluster having some B4 or B_k -like feature is Al_3N_3 : its lowest energy isomer is a hexagonal ring, a planar, D_{3h} , non-buckled structure, in all three levels employed: PIIP potentials [Costales, Blanco, Francisco, Pandey, and Martín Pendás (2005)], and DFT with numerical [Kandalam, Blanco, and Pandey (2001)], and analytical [Costales and Pandey (2003)] basis sets. In the Al_6N_6 case, the lowest energy isomer in all three levels consists of two hexagonal rings in the same chair-like configuration but exchanging Al and N so that inter-layer bonds are of the Al–N type (D_{3d} symmetry). In this case, there is a small buckling with $z = 0.016$ for PIIP potentials [Costales, Blanco, Francisco, Pandey, and Martín Pendás (2005)], and $z = 0.033/0.034$ for DFT calculations, respectively using numerical [Kandalam, Blanco, and Pandey (2002)] and analytical [Costales, Kandalam, and Pandey (2003)] basis sets, to be compared with the experimental B4 phase $z = 0.1128$. The Al_9N_9 lowest energy isomer is again a stacking of alternating Al_3N_3 rings, with D_{3h} symmetry, both employing PIIP potentials and DFT with analytical basis sets [Costales, Blanco, Francisco, Martín Pendás, and Pandey (2006)]. The structure presents a non-buckled central ring, and symmetrical bucklings in the top and bottom rings, amounting to $z = 0.009$ and 0.035 for the PIIP potentials and DFT calculations, respectively. Fi-

nally, although the $Al_{12}N_{12}$ lowest energy structure is a symmetric globular one (in both PIIP potentials and DFT calculations), the second-lowest one is also an alternate stacking of Al_3N_3 rings, in this case with D_{3d} symmetry, in both cases. The bucklings amount to $z = -0.005$ (-0.003) for the inner layer, and to $z = 0.011$ (0.034) for the outer layer in the PIIP potentials (DFT with analytical basis sets) calculations. It is to be noted that the layers buckle in opposite directions, instead of doing it in the same direction as in the bulk material. These results are consistent with those of the slab calculations in the previous Subsection: buckling in small clusters is much smaller than in the B4 phase, becoming almost negligible. Also, all of these structures present non-polar point groups, that is, buckling for the top part is opposite to the buckling of the bottom part, leading to a zero dipole moment. In addition, the buckling is largest for the outer layers, rapidly decreasing and alternating in sign as we proceed to inner layers. The clusters studied with DFT so far are too small, with just one inequivalent inner and outer layer at most. However, these trends are confirmed in the global optimization of larger clusters employing the PIIP potentials [Costales, Blanco, Francisco, Pandey, and Martín Pendás (2005)], where we always found mostly flat inner layers and symmetric bucklings in the outer ones. Although the DFT results presented above, where polarization is not neglected, present somewhat larger bucklings, it seems clear that buckling in finite systems is much smaller than the bulk crystal one. In fact, the driving force towards tetrahedral coordination, and thus to alternate buckling in successive layers, seems to be rather weak in these small clusters; this is clearly a surface effect, trying to avoid three-fold coordinated atoms in the outer layers and the formation of large dipoles.

3.4 Nanostructures

Nanostructures of ionic and semiconductor materials typically display structures almost periodic, with repeating units very similar to the bulk crystal one. This is the case of AlN, where the repeating unit is usually assumed to be that of the B4 bulk phase. In this Subsection, we will present

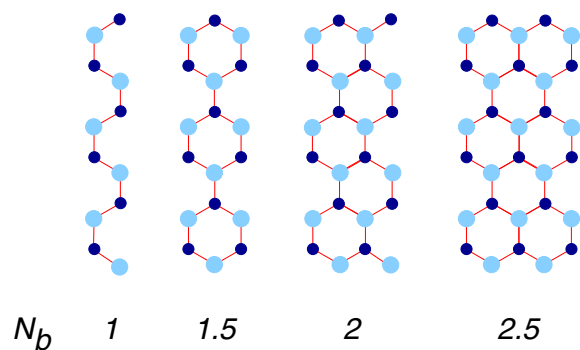


Figure 7: Portions of $N_b = (1, 1.5, 2, 2.5)$ B4-like cells.

first some results concerning full PIIP optimizations of nanobelts (in straight conformations) and nanorings. The initial structure in the optimization of the nanobelts will consist of $N_a \times N_b \times N_c$ repetitions of an orthorhombic unit cell commonly seen in these kind of nanostructures, with cell axes being $2\mathbf{a} + \mathbf{b}$, \mathbf{b} , and \mathbf{c} in terms of the B4 structure ones, having thus twice its volume and $Z = 4$ (see Fig. 1). Along the \mathbf{b} and \mathbf{c} axes, repetitions of $N = (1, 1.5, 2, 2.5)$ will be considered, the half-cell N_b cases being included so the structure has a symmetry plane (see Fig. 7), and the half-cell N_c cases to consider addition of single layers as in the previous Subsection (see Fig. 1). Along the orthorhombic a axis, repetition numbers from 4 to 50 have been considered in this study. The initial structures for nanorings will be generated by bending the nanobelt into a circle, so that the inner layer maintains the bulk-like distances; two possibilities have been considered, having either \mathbf{b} or (more appropriate in comparing with experimental nanorings, see [Kong, Ding, Yang, and Wang (2004)]) \mathbf{c} as the symmetry axis of the ring. However, owing to the rather small repetition numbers considered, the optimization deviates from these structures, in some cases leading to unrelated ones (i.e. globular or amorphous ones). This is something that does not happen for fairly large nanostructures, with larger cohesion and smaller surface-to-bulk ratios. We will present only results for optimizations that maintain their initial structures, so that some periodicity is retained and buckling can be defined.

First, most of the $N_b = 1$ structures, which do not complete any hexagonal ring in the y direction, end up as single-layer nanostructures, and hence will be ignored. Regarding the $N_c = 1$ structures, with just two layers, they tend to open into tube-like (torus-like in the case of rings) structures; those that do not, display bucklings in the range of 0.006 and 0.016. Let us recall that the two-layer small cluster Al_6N_6 had a $z = 0.016$ value obtained using the PIIP potentials. In the rest of the cases, the average z values evolve very slowly with N_a , converging in the range of 10–40 depending on the case considered, ring structures having a slower convergence. Upon N_b increase, convergence is reached for $N_b = 2$, and indeed its z value(s) difference with respect to the $N_b = 1.5$ value(s) is always smaller than 10%. These bucklings are $z = 0.008$ and 0 for the outer and inner layers of $N_c = 1.5$; $z = 0.009$ and -0.002 for the outer and inner layers of $N_c = 2$; and $z = 0.009$, -0.002 , and 0 for the outer, inner, and central layers of $N_c = 2.5$ nanostructures, respectively. These values completely agree with those for Al_9N_9 , and display only a minor deviation for $\text{Al}_{12}\text{N}_{12}$, where the inner layer had a $z = -0.005$ buckling instead of the -0.002 buckling found in the four-layer $N_c = 2$ nanostructures. Given the agreement also found between small clusters and slabs computed using DFT, we believe that all of these results can be extrapolated to other simulation techniques, and that systems finite in the z direction will display consistently comparable bucklings: N atoms sticking out at both extremes, although with a buckling much smaller than the bulk one, an opposite and very small buckling in the next-depth layers, and negligible bucklings in further inner layers.

As previously mentioned, the sizes considered for the full optimization are not too large. The reason for this is that really robust gradient and hessian (or, at least, updated hessian) optimization routines scale with large powers of the number of atoms, N : single-point calculations scale proportionally to N^2 , the optimization memory requirements grow roughly as $9N^2$, and the number of cycles needed in a given optimization increases too, although in a more unpredictable manner.

To simplify the problem, and attending to the near periodicity of the experimental nanostructures, we have previously developed several periodic cluster and nanostructure models. In these models, strict repetition of a given motif is enforced, thus drastically reducing the number of variables. In the periodic cluster model [Francisco (2004); Costales, Blanco, Francisco, Solano, and Martín Pendás (2007)] the motif or unit cell is simply repeated $N_a \times N_b \times N_c$ times; in the periodic nanostructure model, the repetition scheme is superimposed to a deformation of the periodic space, through a coordinate mapping, so that belts (straight ones are equivalent to no mapping) and nanorings (by mapping the $N_a \times N_b \times N_c$ brick into a ring or cylinder crown) can be built in the current implementation [Francisco (2001-2004); Solano (2006)]. This has allowed us to pass from a memory limitation of about 2500 atoms in the full optimizations, to being able to cope with sizes in the range of 30000 or more than 100000 atoms in nanocrystals and nanostructures, respectively. Although the energy evaluation still scales as N^2 , the number of variables is reduced to those in the unit cell, and this can even be further reduced by suitable bulk-like symmetry constraints, hence greatly scaling down the optimization memory and CPU time requirements. This periodicity restriction will in fact help with one of the problems of the full optimizations, namely that after optimization an unintended structure was reached; in this way, although not lowest energy minima, the constrained structures will present smooth size evolutions, while in many cases they will indeed be at least local minima.

The results in these periodic nanostructures are, however, quite simple: either nanobelts, nanorings, or nanocrystals of very different sizes (up to $360 \times 6 \times 6$ testing all N_b and N_c and every 10 values of N_a for belts and rings, and up to $15 \times 15 \times 15$ testing every $k \times k \times k$ value in the nanocrystals) computed with AlN's PIIP potentials lead to zero buckling, $z = 0$. Although it may seem as a problem with central potentials, we have also performed similar calculations with the polarizable SM potentials in nanocrystals of AlN, with the same results. In addition, periodic stacks of (i) al-

ternating Al_3N_3 hexagons, and (ii) hexagonal arrangements of seven such hexagons ($\text{Al}_{12}\text{N}_{12}$ layers), have been examined. The B4-like minima is absent up to about 150 layers for both PIIP and SM potentials, except for the $\text{Al}_{12}\text{N}_{12}$ layers PIIP calculations, in which no minima was found even for our largest 1200 layers calculation; since the thickness of such arrangements is orders of magnitude larger than the trust range of the potentials, the conclusion is still that finite periodic arrangements show no buckling. Thus, the absence of buckling is a consequence of the imposed periodicity: since the finite systems tend to have buckled structures with a σ_z symmetry plane without net dipole, whereas periodicity along the z direction leads to the same buckling in all layers and thus a net dipole $N_a \times N_b \times N_c$ times that in the unit cell, it seems that the compromise situation will be that with $z = 0$, fulfilling both requirements at the same time. This, in fact, agrees with the non-periodic finite systems results within the limits imposed by periodicity. Non-periodic systems had almost negligible buckling for the inner layers, where periodicity was almost fulfilled, having only a small buckling in the outer, frontier layers. In periodicity-enforced systems, geometric surface effects are suppressed, only the energetics of the surface being taken into account; therefore, periodic nanostructures resemble the mostly periodic part of the finite systems studied so far, with zero buckling, and B_k -like.

There have also been hints at B_k -like structures in other simulations from the literature. For example, the B_k structure appears during the course of molecular dynamic simulations of the $B4 \rightleftharpoons B1$ phase transition of small CdSe nanocrystals [Grünwald, Rabani, and Dellago (2006)], using empirical potentials (ionic plus Lennard-Jones form) fitted to reproduce phase parameters and relative energy orderings of the phases involved [Rabani (2002)]. It also appears in [Morgan and Madden (2007)], in which it is the first structure the nanoparticle relaxes into while starting a molecular dynamics simulation from a static B4-like arrangement. However, in this case the kinetic energy of the relaxation makes it overshoot this zero-dipole structure, so it is not clear

whether it is an energy minimum in the generic potentials used in this simulation. The final dynamic structure found was not, in any case, simple B4: it consisted of moderately-sized domains, each of them B4-like, but with opposite buckling in contiguous ones. In this way, the large dipole associated with purely B4-like nanoparticles became quenched in a manner that can be considered alternative to the non-buckling proposed here. Finally, a phase transition into a B_k -like phase has been recently obtained in the simulation of ZnO nanowires under tensile stress along the direction of the hexagonal layers [Kulkarni, Zhou, Sarasamak, and Limpijumng (2006)], clearly supporting the trends found here: although ZnO has a smaller “driving force” towards B_k than AlN (see the discussion above on bulk materials about the definition of this driving force and the discussion on slabs for the larger B_k persistence in AlN than ZnO), the tensile stress enhances this “driving force” and transforms the ZnO wire from B4 into B_k .

4 Conclusions

In this paper we have seen how hexagonal-layered structures, buckled (B4) and non-buckled (B_k), are involved in materials ranging from ionic to semiconductors. In bulk systems, there is a pressure range of simultaneous mechanical stability, which contains an equilibrium pressure, although in these systems it is experimentally masked by the transition into a cubic structure (B1). AlN is one of the systems in which the preference towards the B4 phase is smaller (its close parent BN in fact prefers B_k), and has been the main focus of our calculations. It has been postulated that buckling may play some role in finite systems: polar surfaces are highly energetic, and unfavorable for systems with high surface-to-bulk ratios; the consistent preference for the buckled, polar B4 structure in bulk structures is related to the fact that bulk calculations assume a surfaceless infinite crystal.

Slabs finite along the buckling direction but periodic in the other two, small clusters displaying stacks of hexagonal rings, and nanobelts and nanorings built from B4-like crystal pieces were

considered as examples of finite systems. It was found that, for all of the sizes considered here, buckling was highly quenched as compared with that in the bulk system. In fact, the finite systems displayed a σ_z symmetry plane that led to a zero total dipole, since whatever buckling was present was compensated with that for a symmetric layer on the other side of the finite system. The buckling was small, with N atoms pointing out, in all of the outermost layers, much smaller and opposite to the latter in the next layer, and almost negligible in inner layers. However, by examining the energy-versus-buckling trend for slabs of increasing thickness, it is concluded that there is a turning point for this trend in which the B4-like structures become metastable, and further down they will dominate in the way towards the bulk behavior. This is consistent with other findings in the literature. Thus, it is proposed that the size evolution for these kind of finite systems, nanostructures being particularly important, will present a discontinuity on the slope of size-dependent properties against the nanoparticle size.

It was also found that periodic-like models lead essentially to the correct behavior in nanobelts, nanorings, and nanocrystals. They present zero-buckling due to the periodicity imposed: if the buckling is periodically repeated also along the buckling direction, it is enhanced rather than quenched, and thus a non-buckled zero dipole structure is favored. However, this is indeed the result of non-periodic calculations when the inner layers are considered: buckling is only present in the surface, not in the interior part of the finite system, and hence the main trends in e.g. energetic or elastic properties will be appropriate.

Finally, we would like to point out that “nano” *can* become different from bulk (macroscopic) behavior, but it will be so when “macro” allows for it. That is, the nanostructures can be different from their B4 bulk parent, presenting B_k -like behavior, but this new structure must also be close enough in energy in the bulk regime. The reason for this is that scale introduces new competitors in the “nano” scene (surface energies), but they are not overwhelming: the competition must also be close in the bulk range for these effects to make a

difference in the nanoscale. That is the reason for selecting AlN as the focus material here, which was already found to present an anomalous behavior in our previous nanoscale simulations.

Acknowledgement: The Oviedo group wants to thank the Spanish Ministerio de Educación y Ciencia (MEC) for grant CTQ2006-02976, co-financed by the European Regional Development Fund (FEDER). A. C. wishes to thank the Spanish MEC and the Fondo Social Europeo for her Ramón y Cajal position. C. J. F. S. thanks the Spanish MEC for his F. P. I. grant. We want to thank Prof. John Vail for his kind help with the shell model calculations.

References

- Baiz, P. M.; Aliabadi, M. H.** (2006): Linear buckling analysis of shear deformable shallow shells by the boundary domain element method. *CMES-Computer Modeling in Engineering and Sciences*, vol. 13, pp. 19–34.
- Becke, A. D.** (1988): *Phys. Rev. A*, vol. 38, pp. 3098–100.
- Cai, J.; Chen, N.** (2007): *Phys. Rev. B*, vol. 75, no. 134109.
- Costales, A.; Blanco, M. A.; Francisco, E.; Martín Pendás, A.; Pandey, R.** (2006): First principles study of neutral and anionic (medium-size) aluminum nitride clusters: $Al_n n_n$, $n = 7 - 16$. *J. Phys. Chem. B*, vol. 110, pp. 4092–98.
- Costales, A.; Blanco, M. A.; Francisco, E.; Pandey, R.; Martín Pendás, A.** (2005): Evolution of the properties of $al_n n_n$ clusters with size. *J. Phys. Chem. B*, vol. 109, pp. 24352–60.
- Costales, A.; Blanco, M. A.; Francisco, E.; Solano, C. J. F.; Martín Pendás, A.** (2007): Theoretical simulation of aln nanocrystals. *J. Phys. Chem. C*, vol. xx, pp. xxxx. (submitted).
- Costales, A.; Kandalam, A. K.; Pandey, R.** (2003): Theoretical study of neutral and anion group iii nitride clusters: $m_n n_n$ ($m = al, ga, and in; n = 4-6$). *J. Phys. Chem. B*, vol. 107, pp. 4508–14.
- Costales, A.; Pandey, R.** (2003): Density functional calculations of neutral and negative group iii-nitride clusters. *J. Phys. Chem. A*, vol. 107, pp. 191–97.
- Francisco, E.** (2001-2004): *The Cluster program*. Universidad de Oviedo, 2001-2004.
- Francisco, E.** (2004): *Internal report*. Universidad de Oviedo, 2004.
- Freeman, C. L.; Claeysens, F.; Allan, N. L.; Harding, J. H.** (2006): Graphitic nanofilms as precursors to wurtzite films: Theory. *Physical Review Letters*, vol. 96, no. 066102.
- Freeman, C. L.; Claeysens, F.; Allan, N. L.; Harding, J. H.** (2006): Thin films of wurtzite materials – aln vs. alp. *J. Crystal Growth*, vol. 294, pp. 111–7.
- Frisch, M. J. et al.** (1998): *Gaussian 98*. Gaussian, Inc., Pittsburgh PA, 1998.
- Ghoniem, N. M.; Cho, K.** (2002): The emerging role of multiscale modeling in nano- and micro-mechanics of materials. *CMES-Computer Modeling in Engineering and Sciences*, vol. 3, pp. 147–74.
- Grünwald, M.; Rabani, E.; Dellago, C.** (2006): *Phys. Rev. Lett.*, vol. 96, no. 255701.
- Kandalam, A. K.; Blanco, M. A.; Pandey, R.** (2001): Theoretical study of structural and vibrational properties of $al_3 n_3$, $ga_3 n_3$, and $in_3 n_3$. *J. Phys. Chem. B*, vol. 105, pp. 6080–4.
- Kandalam, A. K.; Blanco, M. A.; Pandey, R.** (2002): Theoretical study of $al_n n_n$, $ga_n n_n$, and $in_n n_n$ ($n = 4, 5, 6$) clusters. *J. Phys. Chem. B*, vol. 106, pp. 1945–53.
- Kong, X. Y.; Ding, Y.; Yang, R. S.; Wang, Z. L.** (2004): Single-crystal nanorings formed by epitaxial self-coiling of polar nanobelts. *Science*, vol. 303, pp. 1348–51.
- Kulkarni, A. J.; Zhou, M.; Sarasamak, K.; Limpijumng, S.** (2006): Novel phase transformation in zno nanowires under tensile loading. *Physical Review Letters*, vol. 97, no. 105502.

Limpijumnong, S.; Lambrecht, W. R. L. (2001): Theoretical study of the relative stability of wurtzite and rocksalt phases in mgo and gan. *Phys. Rev. B*, vol. 63, no. 104103.

Ling, X.; Atluri, S. (2006): A lattice-based cell model for calculating thermal capacity and expansion of single wall carbon nanotubes. *CMES-Computer Modeling in Engineering and Sciences*, vol. 14, pp. 91–100.

Miao, M. S.; Lambrecht, W. R. L. (2003): Unified path for high-pressure transitions of sic polytypes to rocksalt. *Phys. Rev. B*, vol. 68, no. 092103.

Molecular Simulations, Inc. (1995): *DMol user guide, version 2.3.6*, 1995.

Morgan, B. J.; Madden, P. A. (2007): *Phys. Chem. Chem. Phys.*, vol. 9, pp. 2355–61.

Park, J. Y.; Cho, Y.-S.; Kim, S. Y.; Jun, S.; Im, S. (2006): A quasicontinuum method for deformations of carbon nanotubes. *CMES-Computer Modeling in Engineering and Sciences*, vol. 11, pp. 61–72.

Pendás, A. M. (1996): *pairpot3 program documentation*, 1996. (available upon request, angel@fluor.quimica.uniovi.es).

Perdew, J. P.; Wang, Y. (1992): *Phys. Rev. B*, vol. 45, pp. 13244–9.

Rabani, E. (2002): *J. Chem. Phys.*, vol. 116, pp. 258–62.

Saitta, A. M.; Decremps, F. (2004): *Phys. Rev. B*, vol. 70, no. 035214.

Shen, S. P.; Atluri, S. N. (2004): Multiscale simulation based on the meshless local petrov-galerkin (mlpg) method. *CMES-Computer Modeling in Engineering and Sciences*, vol. 5, pp. 235–55.

Solano, C. J. F. (2006): Seminario de Investigación, Universidad de Oviedo, 2006.

Tewary, V. K.; Read, D. T. (2004): Integrated green's function molecular dynamics method for

multiscale modeling of nanostructures: Application to au nanoisland in cu. *CMES-Computer Modeling in Engineering and Sciences*, vol. 6, pp. 359–72.

Vail, J.; Jiang, H. (2006): private communication, 2006.